

A semiconductor-like in-plane junction between overdoped and optimally doped $La_{2-x}Ce_xCuO_4$

Mohsin Rafique(莫辛·拉菲克), Rui Wu(吴蕊), Zefeng Lin(林泽丰), Kui Jin(金魁), Qi-Kun Xue(薛其坤), and Ding Zhang(张定)

Citatio: Chin. Phys. B, 2025, 34 (**9**): 097404. DOI: 10.1088/1674-1056/adda09
http://cpb.iphy.ac.cn; http://iopscience.iop.org/cpb

What follows is a list of articles you may be interested in

Large grain size obtained by substrate directly heating for YBCO epitaxial films

Kebin Li(李珂彬), Yifei Zhang(张一飞), Tong Zhang(张同), Shuguang Yi(易曙光), Shi-Peng Zhang(张世鹏), Quan-Ming Gao(高全明), and Shan-Dong Li(李山东)

Chin. Phys. B, 2025, 34 (**9**): 097403. DOI: 10.1088/1674-1056/add4fc

Synergistic SERS effects in organic/MoS_2 heterojunctions with cavity structure enabling nanoplastics screening and antibiotic adsorption behavior detection

Liqi Ma(马立琪), Abdur Rahim(阿卜杜勒-拉希姆), Baiju Lü(吕白菊), Muhammad Saleem(穆罕默德-萨利姆), Xiaoyu Zhang(张晓雨), Mingyue Li(李明月), Muhammad Zahid(穆罕默德-扎希德), and Mei Liu(刘玫)

Chin. Phys. B, 2025, 34 (**4**): 047402. DOI: 10.1088/1674-1056/ada888

Magnetic flux transitions in two-band single-junction superconductors with time-reversal symmetry breaking

Guo Wang(王果), Tian-Yi Han(韩天意), and Hai Huang(黄海)

Chin. Phys. B, 2025, 34 (**3**): 037401. DOI: 10.1088/1674-1056/ada431

Half-integer Shapiro steps in MgB_2 focused He ion beam Josephson junctions

Dali Yin(殷大利), Xinwei Cai(蔡欣炜), Tiequan Xu(徐铁权), Ruining Sun(孙瑞宁), Ying Han(韩颖), Yan Zhang(张焱), Yue Wang(王越), and Zizhao Gan(甘子钊)

Chin. Phys. B, 2024, 33 (**8**): 087404. DOI: 10.1088/1674-1056/ad4d62

Anomalous spin Josephson effect in spin superconductors

Wen Zeng(曾文) and Rui Shen(沈瑞)

Chin. Phys. B, 2024, 33 (**3**): 037401. DOI: 10.1088/1674-1056/ad1982

A semiconductor-like in-plane junction between overdoped and optimally doped $La_{2-x}Ce_xCuO_4$

Mohsin Rafique(莫辛·拉菲克)[1], Rui Wu(吴蕊)[1,†], Zefeng Lin(林泽丰)[2,3], Kui Jin(金魁)[2,3], Qi-Kun Xue(薛其坤)[1,4,5,6], and Ding Zhang(张定)[1,4,5,7,8]

[1] *Beijing Academy of Quantum Information Sciences, Beijing* 100193, *China*
[2] *Beijing National Laboratory for Condensed Matter Physics, Institute of Physics, Chinese Academy of Sciences, Beijing* 100190, *China*
[3] *School of Physical Sciences, University of Chinese Academy of Sciences, Beijing* 100049, *China*
[4] *State Key Laboratory of Low Dimensional Quantum Physics and Department of Physics, Tsinghua University, Beijing* 100084, *China*
[5] *Frontier Science Center for Quantum Information, Beijing* 100084, *China*
[6] *Southern University of Science and Technology, Shenzhen* 518055, *China*
[7] *RIKEN Center for Emergent Matter Science (CEMS), Wako, Saitama* 351-0198, *Japan*
[8] *Hefei National Laboratory, Hefei* 230028, *China*

(Received 11 March 2025; revised manuscript received 30 April 2025; accepted manuscript online 19 May 2025)

The electron-doped cuprate superconductor exhibits a unique electronic structure, where both electron and hole Fermi surface (FS) pockets coexist in the optimally doped (OP) region, while in the overdoped (OD) region there exists only a large hole FS pocket. It is therefore an intriguing question whether or not a p–n junction arises if the OD electron-doped cuprate interfaces with the OP compound. Here, we construct such an in-plane junction by selectively modulating the doping levels in thin films of $La_{2-x}Ce_xCuO_4$ (LCCO) — a typical electron-doped cuprate. We find that the junction exhibits non-linear, asymmetric *I*–*V* characteristics, which are consistent with those of a p–n semiconductor junction, across a wide temperature range from 250 K to 10 K, regardless of the Hall coefficient sign change or the superconducting transition. We attribute these features to a potential barrier formed at the junction, which is set by the band bending in both OD and OP LCCO.

Keywords: electron-doped cuprate superconductor, ionic liquid gating, junction, transport measurement

PACS: 74.25.F–, 74.72.Ek, 73.40.–c

DOI: 10.1088/1674-1056/adda09 **CSTR:** 32038.14.CPB.adda09

1. Introduction

High temperature cuprate superconductors can be categorized into two families — the hole-doped and the electron-doped compounds.[1,2] While there exist abundant studies on each family,[3–6] the interface between the two families remains scarcely addressed, although it may give rise to exotic properties such as the superconducting diode effect.[7–12] Technically, it is challenging to fabricate such a p–n junction with one side of the copper-oxide layers doped with holes and the other side with electrons. Still, the unique electronic bands of electron-doped cuprates may provide an alternative route toward this goal. In comparison to the hole-doped cuprates which host positive Hall coefficients across the whole phase diagram, the Hall coefficient of electron-doped cuprates can change its sign, from negative to positive, as the doping level varies from the optimally doped (OP) to the overdoped (OD) case.[13] At OP regime, the coexistence of electron and hole Fermi surface (FS) pockets is confirmed in $Nd_{2-x}Ce_xCuO_4$,[14–16] $Pr_{2-x}Ce_xCuO_4$,[17–19] and $La_{2-x}Ce_xCuO_4$ (LCCO)[20,21] through transport and ARPES studies. The interface between OD and OP electron-doped cuprates is therefore expected to mimic a p–n semiconductor junction. Of late, we managed to modulate the doping level of LCCO continuously via ionic liquid gating.[22–25] It was revealed that hydrogen ions were intercalated into the LCCO films as thick as 200 nm. After such a protonation process, LCCO films with a nominal Ce content $x = 0.1$ showed positive Hall coefficients from 10 K to 150 K. This behavior became quantitatively comparable to the OD LCCO with Ce content $x = 0.18$.[26] This result paves one step toward realizing an in-plane p–n junction of cuprates.

Here, we develop an area-selective protonation method to realize an in-plane junction between OD LCCO and OP LCCO. The term "OD LCCO" is nominal, referring to protonated LCCO via ionic liquid gating, which exhibits a temperature-dependent Hall coefficient consistent with that of chemically OD LCCO at $x = 0.18$. We characterize this junction by low temperature electrical measurements. The sheet resistance across the junction is prominently larger than that in either OP LCCO or OD LCCO. Interestingly, the *I*–*V* characteristics across the junction show non-linear behaviors akin to that of a p–n semiconductor junction: a rapid increase of current occurs only after certain threshold voltages are reached. Furthermore, the *I*–*V* characteristic is asymmetric: current

†Corresponding author. E-mail: wu_rui@baqis.ac.cn

© 2025 Chinese Physical Society and IOP Publishing Ltd. All rights, including for text and data mining, AI training, and similar technologies, are reserved.

flowing in the direction from OP LCCO to OD LCCO has a smaller threshold than that in the opposite direction. Such an asymmetry, which is similar to that of a p–n semiconductor junction, persists from 250 K down to 10 K. Our results indicate that there exists band bending across the interface, which is mainly determined by the band structures in both OD and OP LCCO, independent of their Hall coefficient sign.

2. Experimental details

Thin films of LCCO with Ce content $x = 0.1$ were grown on (100)-oriented $SrTiO_3$ (STO) substrates via pulsed laser deposition (excimer KrF laser with a wavelength of 248 nm). Details of the growth recipe were given in our previous reports.[27,28] Two 150-nm-thick samples, labeled S1 and S2, were employed in this study. The superconducting transition temperatures (T_c) of the pristine samples are 25 K and 23 K, respectively. Temperature-dependent resistances were measured using the standard lock-in technique with an AC current of 0.5 μA (13 Hz). Both samples were patterned into Hall bars with a width of 100 μm by using shadow mask Ar^+-ion milling. The Ar^+-ion beam etching was performed using an IBE-KP150 system at an energy of 480 eV with a current density of 0.35 mA/cm^2 for 20 minutes to ensure complete removal of the thin film. To achieve area-selective protonation, half of the Hall bars was covered with either PMMA or AlO_x. A 1-μm-thick PMMA layer (950 kg/mol) was deposited on sample S1 through five cycles of spin coating (4000 rpm) and soft baking (90 °C for 4 minutes) with intermediate cooling steps. Electron-beam lithography (Zeiss Crossbeam 340) was used to define patterned regions for either PMMA removal or AlO_x deposition, enabling selective exposure to the ionic liquid. A 20-nm-thick AlO_x layer was deposited on sample S2 via atomic layer deposition (Ensure Nanotech) using alternating exposures of $Al(CH_3)_3$ and O_3 at a substrate temperature of 80 °C. Electrical contacts were established by pressing indium directly onto the film surface. For the protonation process, we immersed each sample in the ionic liquid, as illustrated in Fig. 1(a). A positive gate voltage was applied to a Pt counter electrode at 300 K to realize the protonation: 1.8 V, 80 min for S1 and 2.6 V, 35 min for S2. The gating condition was optimized for each batch of the samples by carrying out tests on pieces cut from the same 10 mm×10 mm wafer. The gating process intercalated protons into the exposed OP LCCO such that it transformed into the nominal OD LCCO. Figure 1(b) displays this change in doping after gating. Based on our previous study,[22] the Hall coefficient for the protonated LCCO remains positive throughout the temperature range. This behavior is in agreement with that observed for chemically OD LCCO.[26]

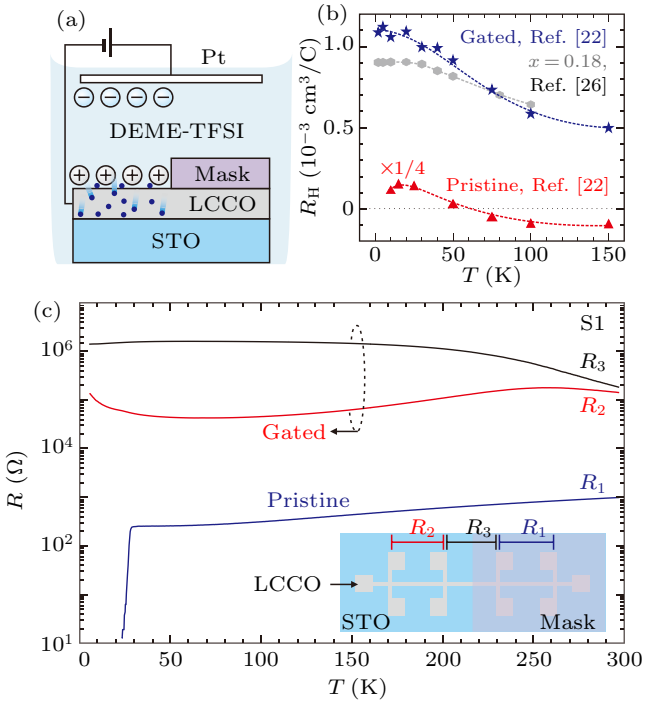


Fig. 1. (a) Schematic drawing of the sample and the experimental setup for realizing area-selective protonation. Dark blue dots represent protons that are intercalated into the exposed LCCO. (b) Temperature-dependent Hall coefficients of pristine OP LCCO with Ce content $x = 0.1$, protonated LCCO after positive gating, and OD LCCO with Ce content $x = 0.18$. The red triangles and blue stars represent the experimental data for pristine and gated samples from Ref. [22], while the gray hexagons represent the experimental data for $x = 0.18$ from Ref. [26]. (c) Temperature-dependent resistances of sample S1. Inset illustrates the Hall bar structure of the sample and the contacts used for measuring R_1, R_2, and R_3. Here, R_1 is measured after deposition of the PMMA/AlO_x masking layer and before gating, and $R_{2,3}$ after gating.

3. Results and discussion

The area-selective protonation effectively establishes an in-plane junction between OD LCCO and OP LCCO. This is supported by the results in Fig. 1(c). The resistance measured in the exposed area after gating, R_2, increases by two orders of magnitude, in comparison to R_1 measured in the masked region (with the same length to width ratio). Also, R_2 decreases from about 250 K to 50 K and slightly increases at lower temperatures. Both the enhanced resistance and the temperature dependence are consistent with those found in our previous study without using the area-selective gating.[22] It indicates that the gated region successfully transits into the nominal OD LCCO. We now investigate the resistance measured from the region hosting the interface between OD LCCO and OP LCCO, R_3. Notably, the temperature-dependent curve of R_3 always hovers above that of R_2. Also, it displays a generally semiconducting trend, in direct contrast to the metallic behavior of R_2, in the same temperature window from 250 K to 50 K. This prominently large resistance suggests the formation of a barrier at the interface, otherwise $R_3(T)$ should closely follow the behavior of $R_2(T)/2$ [since $R_1(T) \ll R_2(T)$].

The I–V characteristics further confirm the formation of a semiconductor-like LCCO junction at the interface. Fig-

ure 2(a) illustrates the measurement setup. We pass a direct current through the Hall bar, with the current flowing from OD LCCO to OP LCCO defined as the positive direction. The four-terminal configuration is employed and the voltage across the junction is registered. Figure 2(b) shows one exemplary *I*–*V* curve measured at 100 K for the OD–OP LCCO junction in sample S1. At this temperature, the Hall effect measurements [Fig. 1(b)] indicate that the OD LCCO behaves as a p-type material with a positive Hall coefficient and OP LCCO as an n-type system. The relatively flat section of the *I*–*V* curve around zero bias corresponds to high resistance observed in the AC transport measurement in Fig. 1(c). Further increasing the voltage above a threshold causes a rapid increase in current. Importantly, the threshold voltage in the positive direction (from OD to OP) is obviously larger than that in the opposite direction (from OP to OD). We point out that this asymmetry is opposite to the naive expectation if treating OD LCCO as a p-type compound and OP LCCO as its n-type counterpart.

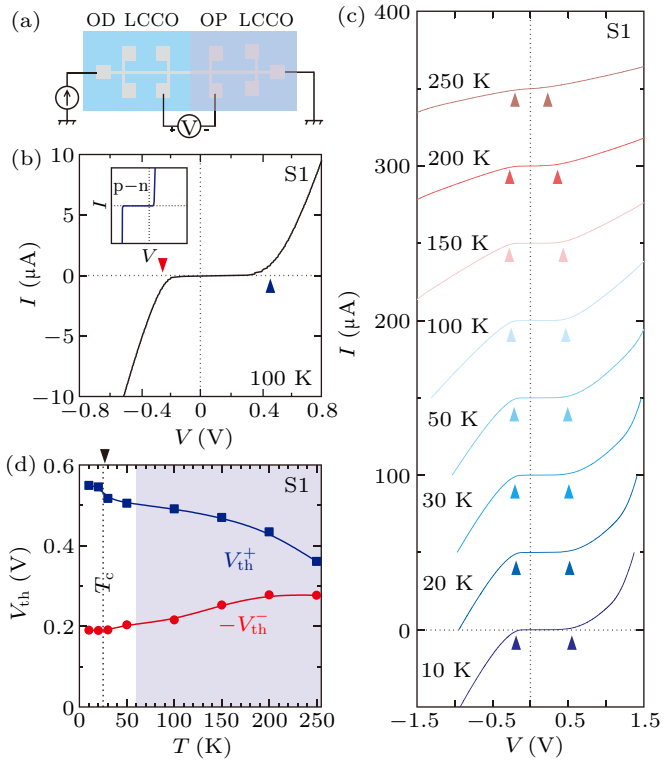


Fig. 2. (a) Schematic drawing of the measurement setup for *I*–*V* characteristics. The current flowing from OD LCCO to OP LCCO is defined as the positive direction. (b) *I*–*V* characteristics of the OD–OP LCCO junction in sample S1 at 100 K. We define the threshold voltage V_{th} as the point (marked by arrows) at which the current reaches 1 μA. The inset illustrates the conventional asymmetric *I*–*V* characteristic of a p–n semiconductor junction. (c) *I*–*V* characteristics of the OD–OP LCCO junction in sample S1 from 250 K to 10 K. V_{th} is marked by arrows. The curves are vertically offset for clarity. (d) Temperature dependences of V_{th} in both current directions for the OD–OP LCCO junction in sample S1. Blue squares indicate the threshold voltages for current flowing from OD LCCO to OP LCCO (V_{th}^{+}), while red circles indicate the threshold voltages for current flowing from OP LCCO to OD LCCO (V_{th}^{-}). The purple and white background regions correspond to OP LCCO with the negative and positive Hall coefficients, respectively. The black arrow denotes T_c. All dotted lines serve as guides to the eye.

The inset of Fig. 2(b) illustrates the conventional asymmetric *I*–*V* characteristic of a p–n semiconductor junction. There, the threshold voltage in the positive direction is obviously smaller. Figure 2(c) presents the *I*–*V* characteristics collected at other temperature points from 250 K to 10 K. It is interesting to note that the same asymmetry persists across the wide temperature range, irrespective of the apparent change of Hall coefficient in OP LCCO [Fig. 1(b)] or the superconducting transition (around $T_c = 25$ K). For a more quantitative analysis, we define the threshold voltage V_{th} as the point [marked by arrows in Fig. 2(b)] at which the current reaches 1 μA in the *I*–*V* curve. Figure 2(d) summarizes the temperature dependences of V_{th} in both current directions. Throughout this temperature range, the threshold voltage for current flowing from OD LCCO to OP LCCO consistently remains larger than that in the opposite direction. Furthermore, the asymmetry becomes more prominent at low temperatures, suggesting a more pronounced band-bending.

Figure 3 illustrates the *I*–*V* characteristics of sample S2 from 100 K to 10 K. We observed asymmetric *I*–*V* behavior again. Here, the threshold is only apparent in the positive direction. In the negative direction, the threshold voltage seems close to zero. This *I*–*V* characteristic is in close analogy to that of an inverted p–n semiconductor junction. In comparisons, sample S1 hosts thresholds in both directions. This contrast seems to be related to the two different recipes employed for masking LCCO. For sample S1, we use PMMA to cover half of the Hall bars. For sample S2, we employ a thin film of AlO_x. The hard mask of AlO_x may be superior than PMMA mask in terms of realizing a sharply defined junction. The PMMA mask, in contrast, may result in certain gradient of doping in the crossover region from OP LCCO to OD LCCO, giving rise to non-Ohmic behavior.

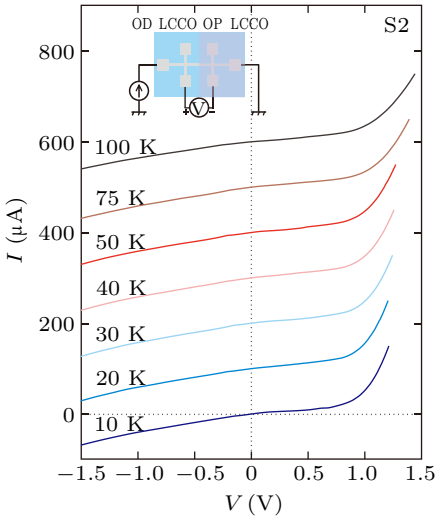


Fig. 3. The *I*–*V* characteristics of the OD–OP LCCO junction in sample S2 from 100 K to 10 K. The inset illustrates a schematic drawing of the measurement setup. The curves are vertically offset for clarity, and all dotted lines serve as guides to the eye.

We now discuss the implications of our experiment. Hall effect measurements indicate that OD LCCO is p-type, while

OP LCCO is n-type. Naively, one might expect that an OD–OP LCCO interface would behave like a p–n semiconductor junction, with a significantly larger threshold voltage when attempting to pass current from OP to OD LCCO. However, the experimentally observed asymmetry is the opposite: passing current from OP to OD encounters a smaller threshold voltage. In fact, the electron-doped cuprate hosts both an electron pocket around $(\pi, 0)$ and a small hole pocket near $(\pi/2, \pi/2)$ in the OP regime, while the OD regime features only a large hole-like FS pocket.[13–21] Based on both the reported experimental results and theoretical calculations,[29–32] we schematically illustrate the band structure of the OD–OP LCCO junction in Fig. 4(a). On the OP LCCO side, the partially filled spectral weight near the Fermi level originates from both an electron-like upper Hubbard band (UHB) and a hole-like band. The UHB and Zhang–Rice singlet are well-separated, with a gap between them. On the OD LCCO side, a single hole-like band extends below the Fermi level, with no gap present. Ionic liquid gating induces protonation in LCCO, driving it into an OD regime of electron-doped cuprates, resulting in an elevated Fermi level for OD LCCO relative to OP LCCO. Consequently, the OD–OP LCCO junction behaves similarly to a p–n semiconductor junction formed from a heavily electron-doped OD region to a lightly electron-doped OP region. In this configuration, the built-in electric field in the LCCO junction points from OD LCCO to OP LCCO, akin to the electric field in a traditional p–n junction that extends from the n-type to the p-type region. Therefore, the band bending from the OD side to the OP side of the LCCO junction is analogous to the band bending observed in p–n semiconductor junctions [from n-type to p-type, as shown in Fig. 4(b)]. This is reflected in the non-linear, asymmetric I–V characteristics of the OD–OP LCCO junction, where current flow from OD LCCO to OP LCCO is less favorable, exhibiting unidirectional conductivity, similar to that of a p–n junction. However, it is evident that the directions of the built-in electric field, band bending, and the asymmetry in the I–V characteristics of the OD–OP LCCO junction are opposite to, or independent of, the expected p–n junction behavior (from OD to OP) as indicated by the Hall coefficient sign. Thus, the electrical behavior of the OD–OP LCCO junction originates from the potential barrier formed by band bending, which is primarily determined by the distinct band structures in the different doping regions of the electron-doped cuprate superconductor. Additionally, the OD–OP LCCO junction exhibits gap-like features around 1 eV in the I–V curves shown in Fig. 2(c), which is notably larger than the smaller chemical potential shift ($\sim$ 100 meV) between the OD and OP regions observed in NCCO.[33] This suggests that the LCCO junction experiences stronger band bending, due to a significant difference in the band structures at both ends of the junction. This disparity is presumed to arise from the varying Hubbard interaction strengths in the electron-doped cuprates across the different doping regions. In other words, the gap-like feature is not simply a result of a chemical potential shift but reflects a more intricate relationship between the electronic states in the OD and OP regions of the LCCO junction.

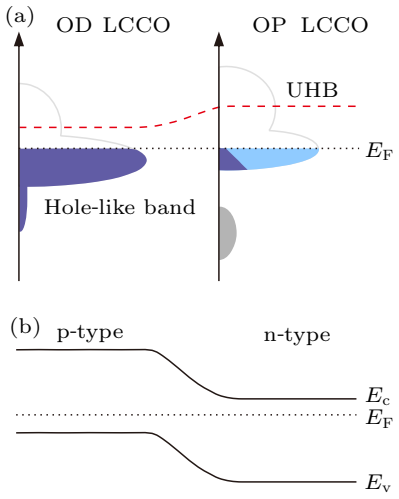


Fig. 4. Schematic drawing of the band structures for an OD-OP LCCO junction (a) and a typical p–n semiconductor junction (b). For OP LCCO in panel (a), the partially filled spectral weight near the Fermi level is contributed by both an electron-like upper Hubbard band (UHB, blue) and a hole-like band (purple). The Zhang–Rice singlet (gray) is well-separated from the UHB, with a gap existing between them. For OD LCCO in panel (a), a single hole-like band (purple) extends below the Fermi level, with no gap present. The red dashed curve illustrates the possible band bending for the LCCO junction. The black dotted lines indicate the Fermi level.

4. Conclusion

In summary, we realized a semiconductor-like in-plane junction consisted of OD LCCO and OP LCCO. The I–V characteristics across the junction reveal nonlinear and asymmetric behavior. Flowing the current from OD LCCO to OP LCCO encounters a larger threshold voltage than driving the current in the opposite direction. This suggests that the potential barrier at LCCO junction originates from the band bending at the interface which is governed by the unique band structures of this electron-doped cuprate.

Acknowledgements

The authors thank valuable discussion with Shusen Ye and Yang Feng. Project supported by the National Key Research and Development Program of China (Grant No. 2022YFA1403100), the National Natural Science Foundation of China (Grant Nos. 52388201, 12361141820, and 12274249), and the Innovation Program for Quantum Science and Technology (Grant No. 2021ZD0302400).

References

[1] Keimer B, Kivelson S A, Norman M R, Uchida S and Zaanen J 2015 *Nature* **518** 179

[2] Zhou X, Lee W S, Imada M, Trivedi N, Phillips P, Kee H Y, Törmä P and Eremets M 2021 *Nat. Rev. Phys.* **3** 462

[3] Yazdani A, da Silva Neto E H and Aynajian P 2016 *Annu. Rev. Condens. Matter Phys.* **7** 11

[4] Proust C and Taillefer L 2019 *Annu. Rev. Condens. Matter Phys.* **10** 409

[5] Fan J Q, Yu X Q, Cheng F J, Wang H, Wang R, Ma X, Hu X P, Zhang D, Ma X C, Xue Q K and Song C L 2022 *Natl. Sci. Rev.* **9** nwab225

[6] Hu S, Qiao H, Gu G, Xue Q K and Zhang D 2024 *Nat. Commun.* **15** 4818

[7] Jiang K and Hu J 2022 *Nat. Phys.* **18** 1145

[8] Zhu Y, Wang H, Wang Z, Hu S, Gu G, Zhu J, Zhang D and Xue Q K 2023 *Phys. Rev. B* **108** 174508

[9] Ghosh S, Patil V, Basu A, Kuldeep, Dutta A, Jangade D A, Kulkarni R, Thamizhavel A, Steiner J F, von Oppen F and Deshmukh M M 2024 *Nat. Mater.* **23** 612

[10] Zhao S Y F, Cui X, Volkov P A, Yoo H, Lee S, Gardener J A, Akey A J, Engelke R, Ronen Y, Zhong R, Gu G, Plugge S, Tummuru T, Kim M, Franz M, Pixley J H, Poccia N and Kim P 2023 *Science* **382** 1422

[11] Ando F, Miyasaka Y, Li T, Ishizuka J, Arakawa T, Shiota Y, Moriyama T, Yanase Y and Ono T 2020 *Nature* **584** 373

[12] Qi S, Ge J, Ji C, Ai Y, Ma G, Wang Z, Cui Z, Liu Y, Wang Z and Wang J 2025 *Nat. Commun.* **16** 531

[13] Armitage N P, Fournier P and Greene R L 2010 *Rev. Mod. Phys.* **82** 2421

[14] Matsui H, Takahashi T, Sato T, Terashima K, Ding H, Uefuji T and Yamada K 2007 *Phys. Rev. B* **75** 224514

[15] Jiang W, Mao S N, Xi X X, Jiang X, Peng J L, Venkatesan T, Lobb C J and Greene R L 1994 *Phys. Rev. Lett.* **73** 1291

[16] Armitage N P, Ronning F, Lu D H, Kim C, Damascelli A, Shen K M, Feng D L, Eisaki H, Shen Z X, Mang P K, Kaneko N, Greven M, Onose Y, Taguchi Y and Tokura Y 2002 *Phys. Rev. Lett.* **88** 257001

[17] Dagan Y, Qazilbash M M, Hill C P, Kulkarni V N and Greene R L 2004 *Phys. Rev. Lett.* **92** 167001

[18] Li P, Balakirev F F and Greene R L 2007 *Phys. Rev. Lett.* **99** 047003

[19] Jin K, Hu W, Zhu B, Kim D, Yuan J, Sun Y, Xiang T, Fuhrer M S, Takeuchi I and Greene R L 2016 *Sci. Rep.* **6** 26642

[20] Jin K, Zhu B Y, Yuan J, Wu H, Zhao L, Wu B X, Han Y, Xu B, Cao L X, Qiu X G and Zhao B R 2007 *Phys. Rev. B* **75** 214501

[21] Jin K, Zhu B Y, Wu B X, Gao L J and Zhao B R 2008 *Phys. Rev. B* **78** 174521

[22] Rafique M, Feng Z, Lin Z, Wei X, Liao M, Zhang D, Jin K and Xue Q K 2019 *Nano Lett.* **19** 7775

[23] Zhang D, Ishizuka H, Lu N, Wang Y, Nagaosa N, Yu P and Xue Q K 2018 *Phys. Rev. B* **97** 184433

[24] Matsuoka H, Nakano M, Uchida M, Kawasaki M and Iwasa Y 2018 *Phys. Rev. B* **98** 144506

[25] Jiang X, Qin M, Wei X, Xu L, Ke J, Zhu H, Zhang R, Zhao Z, Liang Q, Wei Z, Lin Z, Feng Z, Chen F, Xiong P, Yuan J, Zhu B, Li Y, Xi C, Wang Z, Yang M, Wang J, Xiang T, Hu J, Jiang K, Chen Q, Jin K and Zhao Z 2023 *Nat. Phys.* **19** 365

[26] Sarkar T, Mandal P R, Higgins J S, Zhao Y, Yu H, Jin K and Greene R L 2017 *Phys. Rev. B* **96** 155449

[27] Jin K, Butch N P, Kirshenbaum K, Paglione J and Greene R L 2011 *Nature* **476** 73

[28] Yuan J, Chen Q, Jiang K, Feng Z, Lin Z, Yu H, He G, Zhang J, Jiang X, Zhang X, Shi Y, Zhang Y, Qin M, Cheng Z G, Tamura N, Yang Y F, Xiang T, Hu J, Takeuchi I, Jin K and Zhao Z 2022 *Nature* **602** 431

[29] Kusko C, Markiewicz R S, Lindroos M and Bansil A 2002 *Phys. Rev. B* **66** 140513

[30] Moritz B, Schmitt F, Meevasana W, Johnston S, Motoyama E M, Greven M, Lu D H, Kim C, Scalettar R T, Shen Z X and Devereaux T P 2009 *New J. Phys.* **11** 093020

[31] Tanmoy Das, Markiewicz R S and Bansil A 2010 *Phys. Rev. B* **81** 184515

[32] Cédric Weber, Kristjan Haule and Gabriel Kotliar 2010 *Phys. Rev. B* **82** 125107

[33] Harima N, Matsuno J and Fujimori A 2001 *Phys. Rev. B* **64** 220507